INTELLIGENT BEARING FAULT DIAGNOSTIC APPROACH BASED ON MCSA AND DEEP LEARNING

Harida ISSAM*, Bouras ABDELKARIM*, Bouras HICHEM*

*Faculty of Technology, Department of Electromechanical, Electromechanical Systems Laboratory,
Badji Mokhtar University P.O. Box 12, Annaba, 23000, Algeria

issamharida@gmail.com, dr.bourasabdelkarim@gmail.com, hichem.bouras@gmail.com

received 24 October 2025, revised 14 April 2026, accepted 17 May 2026

Abstract: This article presents a new approach to intelligent and efficient fault diagnosis for bearings, which are important mechanical components that are widely used in modern industry. They are are among the most common causes of induction motor failure. Traditional approaches that exploit vibration signals, have several shortcomings, such as the number of intrusive vibration sensors, complex calculations, and limited learning capability. Motor current signature analysis uses a non-intrusive sensor to easily collect stator current signals from a power source. To rapidly process rotating machine failures and automatically provide an accurate diagnosis in the face of increasing condition data, conventional deep neural network models present limitations and inaccurate fault diagnosis results. To overcome this problem, a new intelligent deep learning architecture was proposed. To enhance the predictive capability of our deep neural network model (DNN), we set out to associate specific coefficients to each level and variation, and the results obtained were compared with other models such as support vector machines, k-nearest neighbors, decision tree, long short-term memory (LSTM), and convolutional neural network (CNN). Experimental tests for the early detection of bearing faults under different loads verify the effectiveness of the proposed approach, providing a fast and reliable diagnosis capable of achieving a high diagnostic accuracy that is superior to existing methods.

Key words: deep neural network, induction motor, bearing failure, MCSA, intelligent diagnosis, CNN, LSTM

1. INTRODUCTION

The induction motor (IM) is present in all industrial environments, and is the most commonly used type of motor, due to its robustness and reliability, but it is becoming increasingly complex and technical, which sometimes makes it difficult to perform optimally [1]. It is important to understand that the causes of motor and driving problems are not limited to a single field of expertise. Both mechanical and electrical problems can lead to motor failure. Therefore it is important to arm oneself with good maintenance strategies and tools to avoid costly periods of indisponibility and improve the availability of resources [2]. Bearing health is important for all machines and equipment. Several studies have shown that bearing faults account for 41% of the IM faults. When a bearing failure occurs, it has a cascading effect that significantly increases the risk of motor failure. 13% of motor failures are due to bearing failure, and over 60% of mechanical failures on a site are attributable to bearing wear [3]. Consequently, it is important to learn how to identify the signs before failure.

Accurate real-time fault diagnosis is an important means of ensuring that systems run smoothly [4]. Several failure detection techniques are used in the industrial world [5], the best known being vibration analysis which is a powerful method for diagnosing mechanical defects on rotating machines [6]. It has shown its limits when it comes to defects inducing variations in torque or defects almost imperceptible just at birth. To accurately extract the information related to these failures, the research was particularly directed towards the analysis of the stator currents of the induction motor using motor current signature analysis (MCSA) [7], [8], [9].

In intelligent machine fault diagnosis, the deep learning approach, which is an effective tool for extracting features, has attracted considerable attention from researchers [10]; however traditional artificial intelligence techniques cannot effectively discriminate complex information from raw data [11]. The shallow architectures of artificial neural networks (ANN) limit their ability to learn complex non-linear relationships hidden in measured data [12]. Involved in the data, various deep learning models have been used in fault diagnosis, such as the deep belief network (DBN) [13], [14], long short-term memory (LSTM) [15], the convolutional neural network (CNN) [16], [17] and the deep neural network (DNN) [18], [19], [20].

A multilayer neural network (MLP) is a common type of artificial neural network. It consists of several layers of neurons and is generally organized into three parts: an input layer, several hidden layers, and an output layer [21]. Figure 1 shows an example of a neural network with two hidden layers.

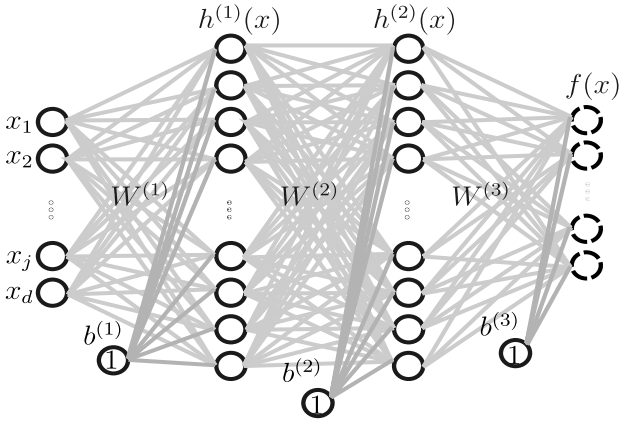

Fig. 1. Two hidden layers neural network

DOI: 10.65731/ama/2026-0039

The following equations describe the operation of a neural network with L hidden layers, where $L+1$ represents the output layer [22].

$$\begin{aligned} &\left(h^{(0)}(X) = X\right) \\ &a^{(k)}(x) = b^{(k)} + W^{(k)}h^{(k-1)}(X) \quad with \quad k > 0 \\ &h^{(k)}(x) = g(a^{(k)}(x)) \quad with \quad k \in \{1, \dots, L\} \\ &h^{(L+1)}(x) = o(a^{(L+1)}(x)) = f(x) \quad with \quad k = L+1 \end{aligned} \tag{1}$$

where: $h^{(0)}(X)$ – represents the activation of the input layer, which is equal to input vector X. This corresponds to the input layer, which makes no transformations to the input data. $a^{(k)}(x)$ – is the pre-activation vector of the hidden layer k, $b^{(k)}$ is the bias term for the hidden layer k, $W^{(k)}$ – is the weight matrix associated with the connections between hidden layer k and hidden layer $(k-1)$, $h^{(k)}(x)$ – represents the activation of the hidden layer k, $g(\cdot)$ and $o(\cdot)$ represent the activation functions applied to the weighted sums of inputs in the hidden layer and output layer respectively, $f(x)$ – represents the final output of the neural network.

The form for updating weights $w_{i,j}$ and biases b_j, and therefore the DNN "Stochastic Gradient Descent (SGD)" learning formulas, is as follows [23]:

$$\begin{aligned} w_{i,j} &\leftarrow w_{i,j} + \alpha a_i \Delta[j] \\ b_j &\leftarrow b_j + \alpha \Delta[j] \end{aligned} \tag{2}$$

with:

$$\Delta[j] = g(z_j)(1 - g(z_j)) \sum_k w_{j,k}\, \Delta[k] \tag{3}$$

Where: α – is the learning rate and $a_i = g(z_i)$ – is the output of neuron i after applying the activation function to the weighted sum of neuron z_i with $g(.)$ – representing the sigmoid activation function.

The most commonly used method for data normalization is the Z-score method [24]. We then used this method to transform the data such that they had a mean of zero and a unit standard deviation. This causes the data distribution to be centered around zero, with a variance of 1. The standardization formula is as follows:

$$X_{std} = \frac{X - \mu}{\sigma} \tag{4}$$

where: X – is the initial value, μ – is the mean of the variable, and σ – is the standard deviation of the variable. In this paper the main contribution to fault diagnosis is the proposal of a new DNN structure designed to process online data of the current signal during load variations which is detected as a fault in classical methods and this by adding to the neural network a specific coefficient for each load, the proposed DNN model is a state of the art choice in this context, it clearly outperforms classical methods and can obtain a more accurate diagnosis with less complex computations.

2. METHODOLOGIE

In this experimental work, we perform diagnostics on an asynchronous motor to detect possible failures. Our approach focuses on the analysis of the single-phase current of the motor to build our dataset, which will later be used to train our deep neural network (DNN) model. Fig. 2 provides an overview of the adopted methodology.

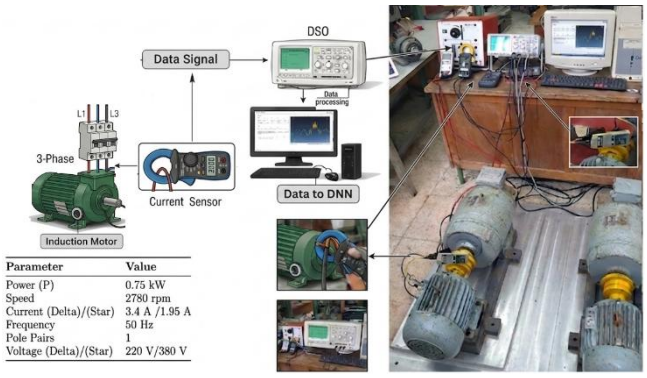

Parameter	Value
Power (P)	0.75 kW
Speed	2780 rpm
Current (Delta)/(Star)	3.4 A /1.95 A
Frequency	50 Hz
Pole Pairs	1
Voltage (Delta)/(Star)	220 V/380 V

Fig. 2. Schematic of the experimental setup and laboratory implementation

To acquire accurate and representative data on electric motor operation under a wide range of conditions, real-time measurements of the electric current in one phase of the motor were collected. Electrical signals were recorded for different operating states of the motor, including a healthy condition and several faulty conditions with deliberately induced bearing defects. The dataset consists of five classes, as illustrated in Table 1, corresponding to current signals acquired from a single phase of an induction motor. Each signal was sampled at 12 kHz and segmented into fixed-length sequences of 4000 samples. These segments represent five bearing conditions: healthy state, ball defect, inner race defect, outer race defect, and cage defect. The data were collected under various load conditions, including no load, 100 W, 200 W, and 300 W, as shown in Fig. 3, Fig. 4, Fig. 5, and Fig. 6, respectively.

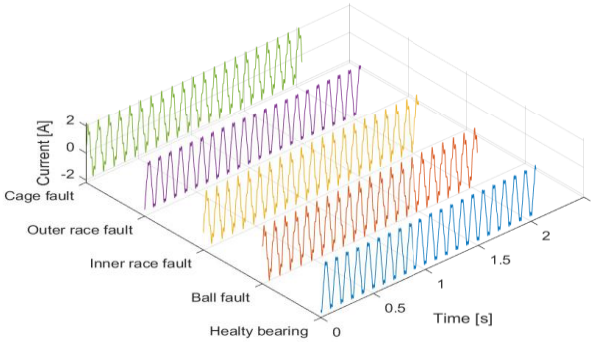

Fig. 3. Signals without load

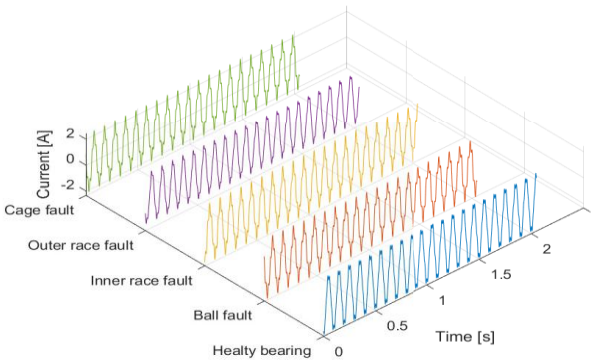

Fig. 4. Signals load 100 Watts

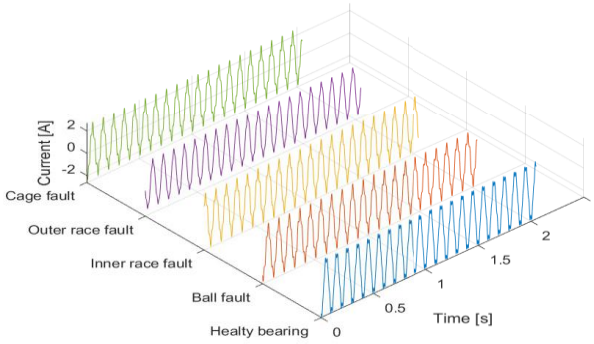

Fig. 5. Signals load 200 Watts

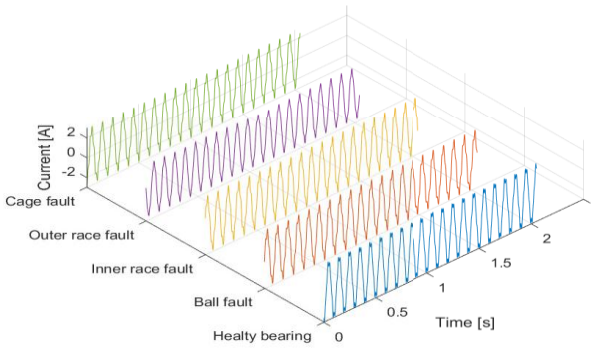

Fig. 6. Signals load 300 Watts

These raw data were subsequently preprocessed and subdivided into 400 segments for each class, as illustrated in Tab. 1.

Tab. 1. Dataset Structure

Load Condition	No load	100 Watts	200 Watts	300 Watts
Classe 1	Healthy	Healthy	Healthy	Healthy
Classe 2	Inner Ring Failure	Inner Ring Failure	Inner Ring Failure	Inner Ring Failure
Classe 3	Outer Ring Failure	Outer Ring Failure	Outer Ring Failure	Outer Ring Failure
Classe 4	Cage Failure	Cage Failure	Cage Failure	Cage Failure
Classe 5	Ball Failure	Ball Failure	Ball Failure	Ball Failure

The "Deep Network Designer" The Deep Network Designer application in MATLAB R2020b was used to design and implement the proposed DNN architecture. The network configuration was defined after extensive empirical tuning of its hyper parameters. Specifically, the number of neurons in the hidden layers was set to 70, the learning rate to 0.001, the number of epochs to 300, and the batch size to 256.

The selection of these hyper parameters was based on a systematic trial-and-error procedure, where multiple combinations were evaluated and compared in terms of classification accuracy and generalization performance on validation data. The final configuration was selected as it consistently achieved the best compromise between high accuracy and stable convergence, while avoiding overfitting.

The input data for the DNN model consist of ten time-domain features extracted from the segments using the Diagnostic Feature Designer application, including the mean, root mean square (RMS), shape factor, kurtosis, skewness, peak value, impulse factor, crest factor, clearance factor, and standard deviation (Std).

To improve interpretability, boxplots of three representative features of RMS, standard deviation (Std), and mean are presented in Fig. 7. These features were selected as illustrative examples from the complete set of extracted features.

As observed, the RMS and Std features exhibit a clear separation between healthy and faulty conditions, indicating their strong discriminative capability. In contrast, the mean feature shows a moderate shift between classes.

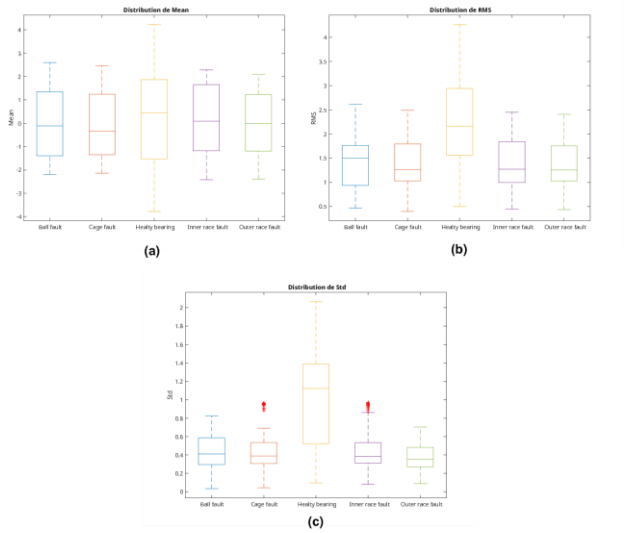

Fig. 7. Distributions of (a) mean, (b) , and (c) RMS standard deviation features for healthy and faulty conditions.

The data were divided into three sets: 70% for training, 15% for validation, and 15% for testing. The DNN model was designed with five outputs to identify bearing conditions. The structure of the model and chosen parameters are listed in Tab. 2.

Tab. 2. Structure of the Deep Neural Network (DNN)

Name	Type	Activation	Parameters
Input	Feature Input	10	-
FC_1	Fully Connected	70	Poids 70×10, Biais 70×1
Batchnorm_1	Batch Normalization	70	Offset 70×1, Scale 70×1
ReLu_1	Rectified linear unit	70	-
FC_2	Fully Connected	70	Poids 70×70, Biais 70×1
Batchnorm_2	Batch Normalization	70	Offset 70×1, Scale 70×1
ReLu_2	Rectified linear unit	70	-
FC_3	Fully Connected	5	Poids 5×70, Biais 5×1
Softmax	Softmax	5	-
Classoutput	Classification Output	-	-

DOI: 10.65731/ama/2026-0039

Fig. 8 illustrates all the steps described above, showing how data are divided, pre-processed and then fed into our DNN model for training.

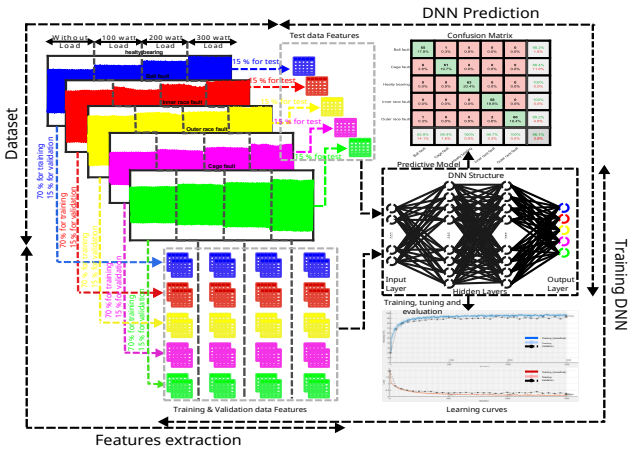

Fig. 8. Rolling bearing fault diagnosis system

To assess the actual performance of our model, we predicted the test data and obtained an accuracy of 96.1%. Fig. 9 shows the confusion matrix, which confirms the robustness of our model for bearing failure classification. We also used our dataset to train other models such as k-nearest neighbors (KNN), vector machines (SVM), decision trees (DT), Convolutional Neural Network (CNN) and Long Short-Term Memory (LSTM) with the aim of comparing them with the DNN model.

The KNN, SVM, and DT models were evaluated using the same test dataset to assess the predictive performance of the DNN model. In contrast, for the CNN and LSTM models, each signal was partitioned into 160 segments per class.

In parallel, the one-dimensional (1D) signal segments were transformed into two-dimensional (2D) scalogram representations using the Continuous Wavelet Transform (CWT) with the Morse wavelet, following the method proposed by [16]. These representations were subsequently used as inputs to the CNN model. Finally, the raw signal segments were directly fed into the LSTM network to capture the temporal dependencies inherent in the data.

Fig. 10, 11, 12, 13, and 14 illustrate the confusion matrices corresponding to the predictions of the KNN, SVM, DT, CNN, and LSTM models, respectively. The quantitative results are summarized in Tab. 3.

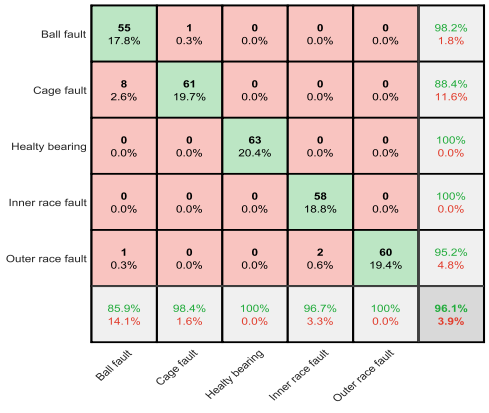

Fig. 9. Confusion Matrix for the DNN Method

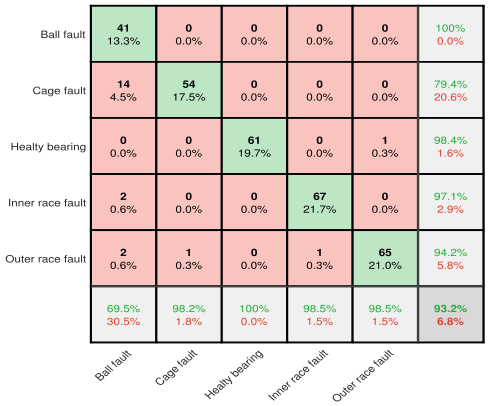

Fig. 10. Confusion Matrix for the KNN Method

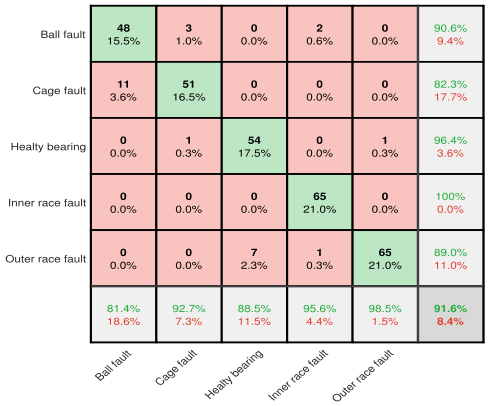

Fig. 11. Confusion Matrix for the SVM Method

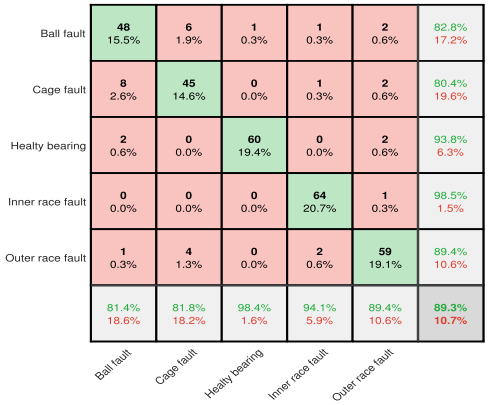

Fig. 12. Confusion Matrix for the DT Method

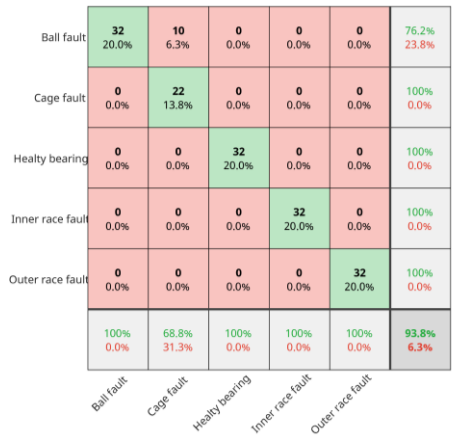

Fig. 13. Confusion Matrix for the CNN Method

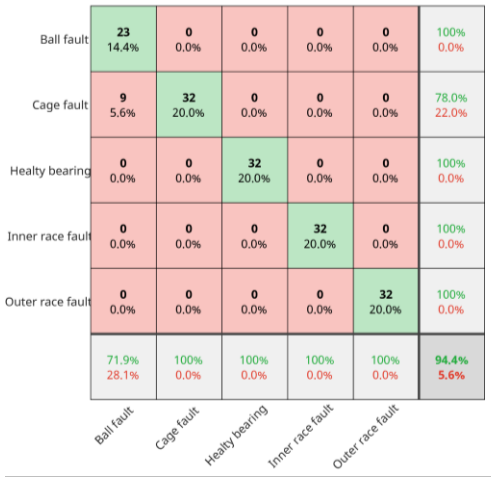

Fig. 14. Confusion Matrix for the LSTM Method

Tab. 3. In-depth comparison of the different methods

Method	Accuracy (%)	Precision (%)	Recall (%)	F1 score (%)
DNN	96,12	96,37	96,20	96,13
KNN	93,20	93,82	92,94	92,62
SVM	91,59	91,66	91,34	91,29
DT	89,32	88,94	89,01	88,95
CNN	93,75	95,24	93,75	93,59
LSTM	94,38	95,61	94,38	94,26

Evidence from this comparative study demonstrates that the DNN architecture is more adept at capturing complex bearing health patterns, resulting in enhanced diagnostic precision.

3. DNN-BASED INTELLIGENT DIAGNOSIS PROPOSED METHOD

When faults occur in the motor, a common manifestation is an increase in the phase current amplitude. However, similar variations may result from normal load changes, making the maximum current feature potentially misleading for fault identification.

To improve the robustness of the DNN model, a coefficient-based normalization is introduced to account for steady-state load levels. Coefficients C_1, C_2, C_3, and C_4 are assigned to no-load, 100 W, 200 W, and 300 W conditions, respectively, enabling the model to distinguish fault-related patterns from load-induced variations.

Assuming a monotonic relationship between load and maximum current under healthy conditions, a Min-Max normalization is applied [25] to define the coefficients as:

$$C_i = 1 + (k-1)\frac{I_{max,i}-I_{min}}{I_{max}-I_{min}} \quad (5)$$

where: I_{min} and I_{max} – are the minimum and maximum current values under fault free conditions. This formulation constrains the coefficients within [1,k] and ensures consistent scaling across load levels.

The parameter k controls the model sensitivity: small values reduce the effect of normalization, while larger values enhance load separation but may amplify noise. A sensitivity analysis shows that moderate values of k provide the best trade-off.

An ablation study further confirms the effectiveness of the proposed approach, demonstrating improved classification performance when the coefficients are included. Fig. 15 illustrates the overall methodology.

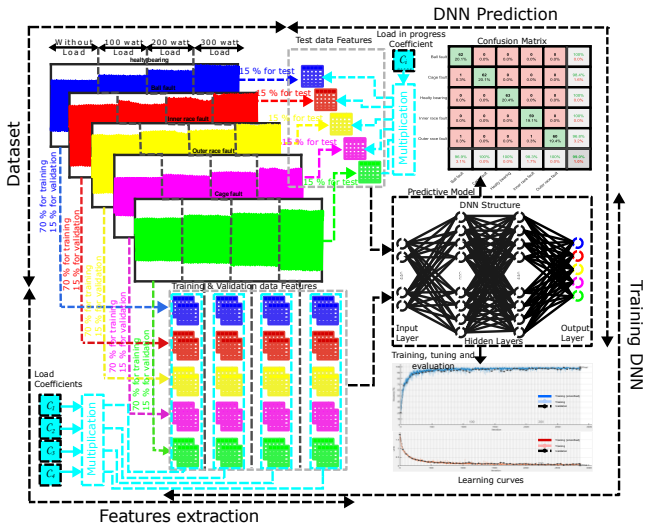

Fig. 15. Architecture of proposed method

After training the DNN model offline, we developed a strategy for online prediction. When new samples are obtained, they are multiplied by the coefficient corresponding to the current load. Fig. 16 illustrates the steps of the online prediction model.

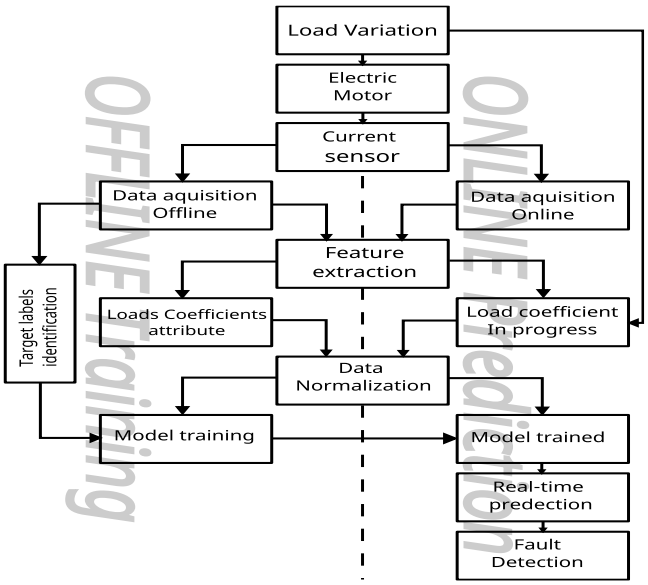

Fig. 16. Flowchart of the proposed method for online diagnosis of an electric motor

4. EXPERIMENTAL RESULTS AND ANALYSIS

The results obtained using the proposed method are satisfactory. Fig.17 shows the results under the confusion matrix, confirming the effectiveness of the proposed method, with class identification now correct. The accuracy of the model increased from 96.1% to 99.0% using the same training and test data, ensuring a fair comparison of the performance before and after the

DOI: 10.65731/ama/2026-0039

application of the proposed method. In addition, the learning curve underwent significant improvement, demonstrating a better adaptation of the model to the pre-processed training data.

The proposed method was applied to KNN, SVM, DT, CNN, and LSTM models. The results obtained, compared with conventional methods, are significantly more satisfactory.

For the KNN method (Fig. 18), the accuracy increased from 93.2% to 98.7%. For the SVM method (Fig. 19), the accuracy improved from 91.6% to 96.8%. Similarly, for the DT method (Fig. 20), the accuracy rose from 89.3% to 97.7%.

For the CNN method (Fig. 21), the accuracy increased from 93.8% to 98.1%, while for the LSTM method (Fig. 22), it improved from 94.4% to 98.8%.

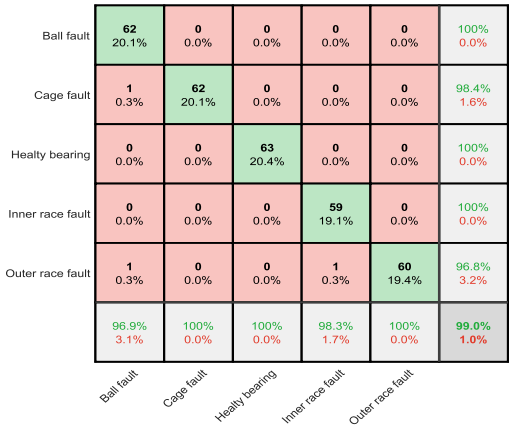

Fig. 17. Confusion Matrix for the DNN Proposed Method

Fig. 18. Confusion Matrix for the KNN Proposed Method

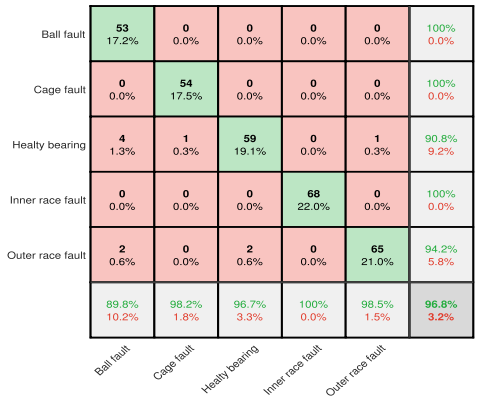

Fig. 19. Confusion Matrix for the SVM Proposed Method

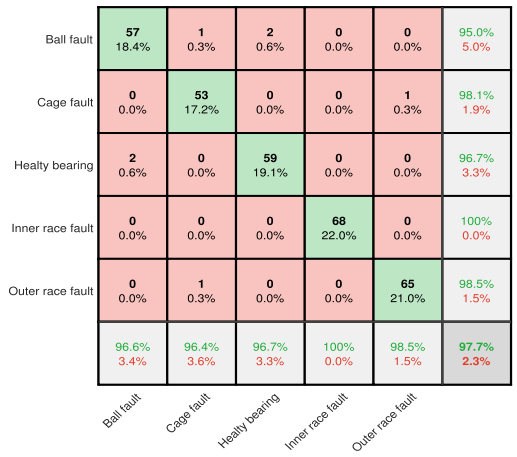

Fig. 20. Confusion Matrix for the DT Proposed Method

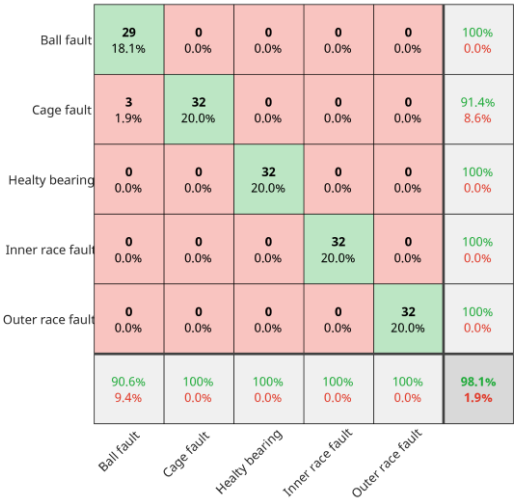

Fig. 21. Confusion Matrix for the CNN Proposed Method

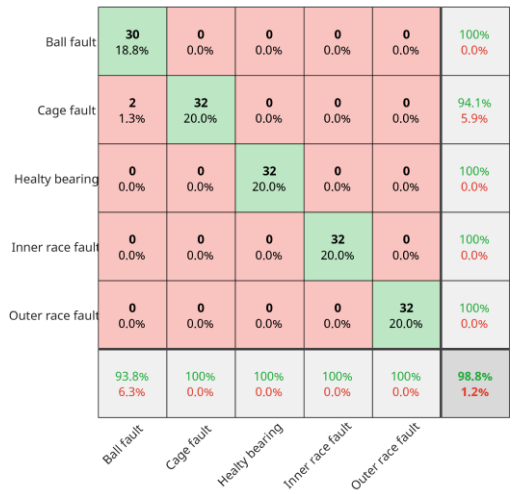

Fig. 22. Confusion Matrix for the LSTM Proposed Method

Fig. 23 shows a comparison of the different methods before and after using the proposed approach. Tab. 4 presents a more in-depth analysis and a detailed comparative performance evaluation.

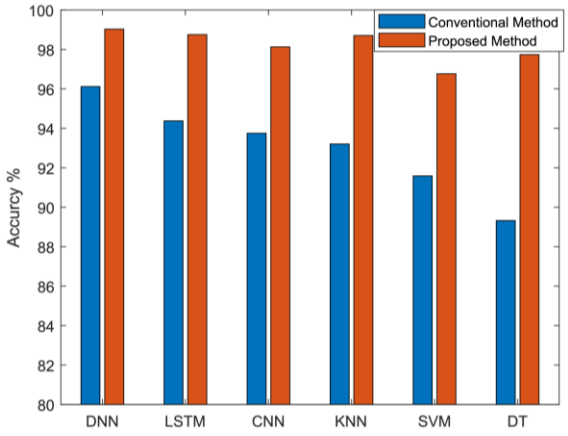

Fig. 23. Comparison of proposed and conventional methods

Tab. 4. In-depth comparison of the different methods

Method	Accuracy (%)	Precision (%)	Recall (%)	F1 score (%)
DNN	96,12	96,37	96,20	96,13
DNN (Proposed)	99,03	99,04	99,04	99,03
***k*-NN**	93,20	93,82	92,94	92,62
***k*-NN (Proposed)**	98,71	98,65	98,69	98,66
SVM	91,59	91,66	91,34	91,29
SVM (Proposed)	96,76	96,99	96,64	96,73
DT	89,32	88,94	89,01	88,95
DT (Proposed)	97,73	97,67	97,64	97,65
CNN	93,75	95,24	93,75	93,59
CNN (Proposed)	98,13	98,29	98,13	98,12
LSTM	94,38	95,61	94,38	94,26
LSTM (Proposed)	98,75	98,82	98,75	98,75

5. CONCLUSION

Diagnosis and predictive detection of electric motor faults are essential, and an automatic, online detection solution is the most practical way to achieve this. This is possible owing to diagnostics using artificial intelligence methods. Our work involved the application of an online intelligent diagnostic method to an asynchronous motor for the detection of bearing faults. Several techniques have been employed, including support vector machines (SVM), k-nearest neighbors (KNN), decision trees (DT), convolutional neural network (CNN) and long short-term memory (LSTM) with the aim of comparing them with the deep neural networks (DNN) model.

The approach consisted of using the current of a phase to extract the characteristics of this signal and, then using it as input for our models. The DNN model was then trained to detect and identify the bearing defects under different loads. A comparison was then made between the KNN, SVM, DT, CNN, and LSTM methods.

The proposed method demonstrates significant effectiveness in mitigating the confusion between load variations and fault signatures. To this end, a coefficient-based normalization strategy was implemented, leading to a substantial improvement in model performance. In particular, the accuracy of the best-performing DNN model increased from 96.1% to 99.0%. Substantial gains were also observed for the other models, with improvements from 93.2% to 98.7% for KNN, from 91.6% to 96.8% for SVM, from 89.3% to 97.7% for DT, from 93.8% to 98.1% for CNN, and from 94.4% to 98.8% for LSTM.

The results confirm the effectiveness of the proposed approach for fault detection by current analysis, based on a non-intrusive sensor that enables continuous monitoring without interrupting or modifying the system. The precise identification of fault classes enhances the reliability of diagnostics and predictive maintenance. Future work will focus on validation in a real-world industrial environment, with an emphasis on optimizing computational costs and simplifying integration into existing monitoring systems to ensure robustness and economic viability at scale.

REFERENCES

1. Niyongabo J, Zhang N-Dikumagenge. Bearing fault detection and diagnosis based on densely connected convolutional networks. Acta Mech Autom. 2022;16(2):133–135. https://doi.org/10.2478/ama-2022-0017
2. Benbouzid MEH. A review of induction motors signature analysis as a medium for faults detection. IEEE Trans Ind Electron. 2000;47(5):984–993. https://doi.org/10.1109/41.873206
3. Schoen RR, Habetler TG, Kamran F, Bartfield R. Motor bearing damage detection using stator current monitoring. IEEE Trans Ind Appl. 1995;31(6):1274–1279. https://doi.org/10.1109/28.475697
4. Seera M, Lim CP, Ishak D, Singh H. Offline and online fault detection and diagnosis of induction motors using a hybrid soft computing model. Appl Soft Comput. 2013;13(12):4493–4507. https://doi.org/10.1016/j.asoc.2013.08.002
5. Jimenez GA, Munoz AO, Duarte-Mermoud MA. Fault detection in induction motors using Hilbert and wavelet transforms. Electr Eng. 2007;89:205–220. https://doi.org/10.1007/s00202-005-0339-6
6. Huang F, Chen C, Wang Z, Fu H. Research on vibration characteristics of permanent magnet synchronous motor rotor parallel eccentricity and bearing inner ring radial misalignment coupling fault. Electr Eng. 2025;1–23. https://doi.org/10.1007/s00202-025-02949-4
7. Bouras A, Bouras S, Kerfali S. Prediction of the mass unbalance of a variable speed induction motor by stator current multiple approaches. Turk J Electr Eng Comput Sci. 2018;26(2):1056–1068. https://doi.org/10.3906/elk-1702-58
8. Corne B, Vervisch B, Debruyne C, Knockaert J, Desmet J. Comparing MCSA with vibration analysis in order to detect bearing faults—a case study. In: IEEE International Electric Machines & Drives Conference. Coeur d'Alene. ID USA. 2015;1366–1372. https://doi.org/10.1109/IEMDC.2015.7409240
9. Li C, Afshar M, Akin B. Fault detection in small fan motors using MCSA. In: IEEE International Electric Machines & Drives Conference. San Francisco. CA USA. 2023; 1–7. https://doi.org/10.1109/IEMDC55163.2023.10238848
10. Zhang S, Zhang S, Wang B, Habetler TG. Deep learning algorithms for bearing fault diagnostics—a comprehensive review. IEEE Access. 2020;8:29857–29881. https://doi.org/10.1109/ACCESS.2020.2972859
11. Neupane D, Seok J. Bearing fault detection and diagnosis using Case Western Reserve University dataset with deep learning approaches: A review. IEEE Access. 2020;8:93155–93178. https://doi.org/10.1109/ACCESS.2020.2990528
12. Li B, Chow M-Y, Tipsuwan Y, Hung JC. Neural-network-based motor rolling bearing fault diagnosis. IEEE Trans Ind Electron. 2000;47(5):1060–1069. https://doi.org/10.1109/41.873214
13. Zhu J, Hu T, Jiang B, Yang X. Intelligent bearing fault diagnosis using

DOI: 10.65731/ama/2026-0039

PCA-DBN framework. Neural Comput Appl. 2020;32:10773–10781. https://doi.org/10.1007/s00521-019-04612-z
14. Gao S, Xu L, Zhang Y, Pei Z. Rolling bearing fault diagnosis based on SSA optimized self-adaptive DBN. ISA Trans. 2022;128:485–502. https://doi.org/10.1016/j.isatra.2021.11.024
15. Sabir R, Rosato D, Hartmann S, Gühmann C. LSTM based bearing fault diagnosis of electrical machines using motor current signal. In: 18th IEEE International Conference on Machine Learning and Applications. Boca Raton. FL USA. 2019; 613–618. https://doi.org/10.1109/ICMLA.2019.00113
16. Boudiaf R, Abdelkarim B, Issam H. Bearing fault diagnosis in induction motor using continuous wavelet transform and convolutional neural networks. Int J Power Electron Drive Syst. 2024;15(1):591–602. https://doi.org/10.11591/ijpeds.v15.i1.pp591-602
17. Guo Z, Yang M, Huang X. Bearing fault diagnosis based on speed signal and CNN model. Energy Rep. 2022;8(13):904–913. https://doi.org/10.1016/j.egyr.2022.08.041
18. Zhao X, Jia M. A new local-global deep neural network and its application in rotating machinery fault diagnosis. Neurocomputing. 2019;366:215–233. https://doi.org/10.1016/j.neucom.2019.08.010
19. Gangsar P, Bajpei AR, Porwal R. A review on deep learning based condition monitoring and fault diagnosis of rotating machinery. Noise Vib Worldw. 2022;53(11):550–578. https://doi.org/10.1177/09574565221139638
20. Pandiyan M, Babu TN. Systematic review on fault diagnosis on rolling-element bearing. J Vib Eng Technol. 2024;1–35. https://doi.org/10.1007/s42417-024-01358-4
21. Alzubaidi L, et al. Review of deep learning: Concepts, CNN architectures, challenges, applications, future directions. J Big Data. 2021;8:1–74. https://doi.org/10.1186/s40537-021-00444-8
22. Islam MM, Murase K. A new algorithm to design compact two-hidden-layer artificial neural networks. Neural Netw. 2001;14(9):1265–1278. https://doi.org/10.1016/S0893-6080(01)00075-2
23. Zhang S, Zhang C, You Z, Zheng R, Xu B. Asynchronous stochastic gradient descent for DNN training. In: IEEE International Conference on Acoustics, Speech and Signal Processing. Vancouver BC Canada. 2013; 6660–6663. https://doi.org/10.1109/ICASSP.2013.6638950
24. Abdullah NF, Rashid N, Othman KA, Musirin I. Vehicles classification using z-score and modelling neural network for forward scattering radar. In: 15th International Radar Symposium. Gdansk Poland. 2014; 1–4. https://doi.org/10.1109/IRS.2014.6869280
25. Henderi H, Wahyuningsih T, Rahwanto E. Comparison of min-max normalization and z-score normalization in the k-nearest neighbor (kNN) algorithm to test the accuracy of types of breast cancer. Int J Informatics Inf Syst. 2021;4(1):13–20. https://doi.org/10.47738/ijiis.v4i1.73

Harida Issam: https://orcid.org/0009-0008-7498-407X

Bouras Abdelkarim: https://orcid.org/0000-0002-0836-8200

Bouras Hichem: https://orcid.org/0009-0006-7262-8106